AUTOMATIC TARGET DETECTION ON TUCKER DECOMPOSED HYPERSPECTRAL IMAGES

Augustine Koh, Jingting Zhou, Ken-Yoong Lee, Asha Vijayakumar
EADS Innovation Works South Asia
110 Seletar Aerospace View, Singapore
Tel: +65 6592 7300; Fax. +65 66591276
E-mail: {ken-yoong.lee, asha.vijaya-kumar}@eads.net,

KEY WORDS: Hyperspectral Imagery, Tucker decomposition, principal component analysis, Reed-Xiaoli detector (RXD), Uniform target detector (UTD), Nested Spatial Window-based Detector (NSW).

Abstract: Hyperspectral imaging has become one of the most promising and emerging technologies in remote sensing. It has made great advances in recent years by the introduction of new techniques, to take advantage of the vast amount of information contained within hyperspectral images (HSIs). However, the increase in the information comes at the expense of higher computational cost in processing the data. In this work, we measure the target detection accuracy on the Tucker decomposed hyperspectral images. A comparison of PCA reduced and Tucker reduced data is also drawn. The effectiveness of target detection on Tucker decomposed data is explicitly shown on AisaEagle dataset (Wadstromer *et al.*, 2010) using RX detector.

1. INTRODUCTION

Hyperspectral imaging sensors measure the radiance of objects among a large number of continuous wavelength bands and generate hyperspectral images (HSI) resulting in more information gathered compared to multispectral imaging. But the huge amount of data acquired increases the computational cost of processing and might also decrease the target detection accuracy (Landgrebe, 2002). Thus, dimensionality reduction becomes a crucial step.

A number of methods have been suggested for this purpose, namely Principal Component Analysis (PCA) (Farrell and Mersereau, 2005) and Independent Component Analysis (ICA). PCA maximizes the amount of data variance by orthogonal projection and is the simplest and most common approach for dimension reduction. ICA is a higher-order method that seeks linear projections which are nearly statistically independent but not necessarily orthogonal to each other. However, both methods neglect the combined spatial and spectral correlation of the dataset. In contrast, tensor decomposition simultaneously takes into account the spatial and the spectral correlation of HSIs (Renard and Bourennane, 2008). Tucker decomposition is one of the most popular tensor decompositions. In Karami *et al.*, (2011a) and Karami *et al.*, (2012b) the authors have shown the effectiveness of Tucker decomposition for compression and noise reduction in HSIs.

In this work, we explore the effectiveness of Tucker decomposition of HSIs in the context of target detection. We also compare the chosen decomposition approach with other dimensionality reduction techniques like PCA. A large number of hyperspectral detection algorithms have been developed (Manolakis and G. Shaw, 2002) which can be broadly classified into two types: one is based on knowledge of the target's signature while the other locates target by elimination of the background, more commonly known as anomaly detection (Stein *et al.*, 2002). Three anomaly detection algorithms, namely RXD, RX-UTD (Ashton and Schaum, 1998) and NSW-DW (Liu and Chang, 2004), were implemented on the dimension reduced dataset.

2. DIMENSION REDUCTION-TUCKER DECOMPOSITION

Hyperspectral data has two types of redundancies: spatial and spectral redundancies. Hence dimension reduction is an important step to reduce data volume especially for on-board processing, maintaining detection accuracy. However, PCA is applied on vectorized images, thereof, the spatial information is lost. Hyperspectral image is a three dimensional matrix known as a tensor array. Tucker decomposition allows direct principal component analysis on multidimensional array (Tucker, 1966). In the context of hyperspectral imagery, this decomposition performs joint spatial and spectral processing.

Tucker decomposition of an hyperspectral image $\boldsymbol{\mathcal{X}} \in \mathbb{R}^{I_1 \times I_2 \times I_3}$ can be expressed as,

Here, $\boldsymbol{U}^{(1)} \in \mathbb{R}^{I \times K_1}$, $\boldsymbol{U}^{(2)} \in \mathbb{R}^{J \times K_2}$, and $\boldsymbol{U}^{(3)} \in \mathbb{R}^{K \times K_3}$ are the factor matrices (which are usually orthogonal) and can be viewed as the principle components in each mode. The tensor $\boldsymbol{\mathcal{G}} \in \mathbb{R}^{K_1 \times K_2 \times K_3}$ is called the *core tensor* and its elements show the degree of interaction among different components.

The objective is to decompose the original tensor $\boldsymbol{\mathcal{X}}$ of size $I_1 \times I_2 \times I_3$ into a core tensor $\boldsymbol{\mathcal{G}}$ of size $K_1 \times K_2 \times K_3$ and three subspaces $\boldsymbol{U}^{(1)}, \boldsymbol{U}^{(2)}, \boldsymbol{U}^{(3)}$ by solving the minimization problem using alternate least square algorithm (De Lathauwer *et al.*, 2000),

$$\min_{\boldsymbol{\mathcal{G}}, \mathbf{U}^{(n)}} \left\| \boldsymbol{\mathcal{X}} - \boldsymbol{\mathcal{G}} \times_1 \mathbf{U}^{(1)} \times_2 \mathbf{U}^{(2)} \times_3 \mathbf{U}^{(3)} \right\|_{\mathbf{F}}^2, \tag{2}$$

subject to $\boldsymbol{\mathcal{G}} \in \mathbb{R}^{K_1, K_2, K_3}$, $\boldsymbol{U}^{(n)} \in \mathbb{R}^{I_n \times K_n}$ and columnwise orthogonal for $n = 1,2,3$.

3. TARGET DETECTION

Anomaly detection is chosen frequently as the preferred detection approach since no prior knowledge of the target's signature is needed. We compare the performance of three anomaly detectors namely RXD, UTD, RX-UTD and NSW using data that was reduced in dimensionality using Tucker decomposition.

A generalized likelihood ratio test is the foundation for anomaly detection algorithms. Thresholding the likelihood ratio provides the hypothesis test that satisfies various optimality criteria including: maximum probability of detection for a given probability of false alarm. The key assumptions of RXD are that the background and the target can be modeled by multivariate Gaussian distribution with the same spectral covariance, i.e. it is assumed that the background mean is the global mean while the target mean is unknown (Manolakis e*t al.*, 2009 and Chang and Chiang, 2002). The competitive hypotheses are:

$$\boldsymbol{H_0}: \boldsymbol{x} \sim \boldsymbol{N_p}(\boldsymbol{\mu_b}, \sum_{\boldsymbol{b}}) \tag{3}$$

$$\boldsymbol{H_1}: \boldsymbol{x} \sim \boldsymbol{N_p}(\boldsymbol{\mu_t}, \sum_{\boldsymbol{t}}) \tag{4}$$

where $\boldsymbol{\mu_b}, \boldsymbol{\mu_t}$ denote the mean vectors of the background and the target, respectively: $\sum_b$, $\sum_t$ denote the $p \times p$ covariance matrices of the background and the target, respectively. The maximum likelihood estimate of $\boldsymbol{\mu_t}$, denoted as $\hat{\boldsymbol{\mu}}$, under the H_1 hypothesis is given by $\hat{\boldsymbol{\mu}} = \boldsymbol{x}$.

The RX detector is a constant false alarm rate (CFAR) detector for anomaly detection proposed by Reed-Xiaoli (Reed and Yu, 1990). Targets whose signatures are distinct from their surroundings with no *a-priori* knowledge are detected. This is done by calculating the Mahalanobis Distance by considering the spectral covariance matrix of the image and then detecting anomalies through thresholding. Suppose that L is the number of spectral bands and $\boldsymbol{x_i}$ is an L × 1-column pixel vector in a hyperspectral image and the image contains N pixels. Then the RXD implements a filter specified by,

$$\boldsymbol{\delta_{RXD}}(\boldsymbol{x_i}) = (\boldsymbol{x_i} - \boldsymbol{\mu})^{\boldsymbol{T}} \boldsymbol{K}_{\boldsymbol{L \times L}}^{-\boldsymbol{1}} (\boldsymbol{x_i} - \boldsymbol{\mu}) \tag{5}$$

$$\boldsymbol{K_{L \times L}} = \sum_{\boldsymbol{i=1}}^{\boldsymbol{N}} (\boldsymbol{x_i} - \boldsymbol{\mu})(\boldsymbol{x_i} - \boldsymbol{\mu})^{\boldsymbol{T}}, \tag{6}$$

where $\boldsymbol{\mu}$ is the global sample mean and $\mathbf{K}_{\mathrm{L \times L}}$ is the sample covariance matrix of the image. $\boldsymbol{\delta}_{\mathrm{RXD}}(\mathbf{x_i})$ is the Mahalanobis distance.

The images generated by RXD are usually grayscale, where brighter gray levels are considered to be anomalous (target) pixels. As background pixels are assumed to be homogenous, target pixels should behave as outliers, falling in the right tail of the image's grayscale distribution (Chang and Chiang, 2002). The targets are differentiated from the background by automatic thresholding. A histogram plot of the image is used to define the rejection probability for a given gray scale value α,

$$\boldsymbol{P(\alpha)} = \boldsymbol{Pr}\,(\boldsymbol{\delta_{RXD}}(\boldsymbol{x_i}) < \alpha), \tag{7}$$

Then, a threshold α_0 for detecting the anomalies is determined by setting a confidence coefficient γ such that $\mathrm{P}(\alpha_0) = \gamma$. If $\boldsymbol{\delta}_{\mathrm{RXD}}(\boldsymbol{x_i}) > \alpha_0$, then $\boldsymbol{x_i}$ is detected as anomaly. In this work, an estimation of the number of target pixels is assumed to be known, and set to $1 - \gamma = \frac{\text{\# of target pixels}}{\text{\# of pixels in an image}}$. The same thresholding method is also applied to the other detection algorithms RXD-UTD and NSW evaluated in this paper. In RXD-UTD, Ashton and Schaum, (1998) suggest that background subtraction could enhance the RXD detection performance, which indicates that incorporating UTD into RXD may remove the background and therefore improve performance as well. The idea in NSW-DW (Liu and Chang, 2004) is to use a nested three windows where the inner and middle windows are to

extract targets with smallest size and largest size respectively, while the outer window is to describe the background.

4. EXPERIMENTS AND RESULTS

The hyperspectral dataset used for validation in this study was provided by the Swedish Defence Research Institute (FOI) (Wadstromer *et al.*, 2010). The spectral resolution is about 10nm and covers the visual and near infrared range from 0.39 μm to 0.96 μm with 60 spectral bands. The scene shows an edge of a wood, an open field, and rough open terrain, with six target military and civilian vehicles placed at various locations within the image.

Fig. 2 shows the results of dimension reduction using PCA and Tucker on the dataset. A comparison of the performance is objectively measured by the target detection accuracy. Anomaly detection was performed using a RX detector. Initially, the optimum number of spatial ranks required by Tucker was established by carrying out various combinations of the spatial ranks K_1 and K_2. The results in Fig. 3 show that $K_1 = K_2 = 100$ yielded the best detection accuracy. The number of spectral components corresponding to the best detection accuracy for PCA and Tucker is 30. Therefore RXD, is applied to both PCA and Tucker containing the first 30 spectral principal components. It can be observed that the accuracy of detection is not affected by the significant reduction in the spectral components.

A comparison of the detection accuracy measurement is done on raw images and images after dimension reduction using PCA and Tucker. The detection is a two-class prediction problem: the pixels in an image are either labeled as target (positive-p) or background (negative-n). Hence, there are four possible outcomes from a binary detector: True Positive (TP) - if the outcome from a prediction is p and the actual value is also p; False Positive (FP) - if the outcome from a prediction is p, while the actual value is instead n; True Negative (TN) - if the outcome from a prediction is n and the actual value is also n; False Negative (FN) - if the outcome from a prediction is n, while the actual value is instead p. The four outcomes can be formulated in a 2×2 confusion matrix:

prediction outcome \ actual value	*p*	*n*	total
p'	True Positive	False Positive	P'
n'	False Negative	True Negative	N'
total	P	N	

and four measurement results can be attained for this confusion matrix given as recall rate TP/(TP+FN), precision TP/(TP+FP), accuracy (TP+TN)/(P+N) and the false alarm rate FP/(FP+TN).

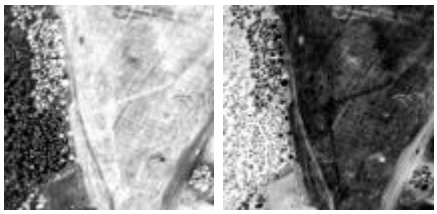

Channel One

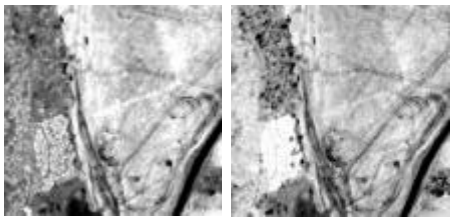

Channel Two

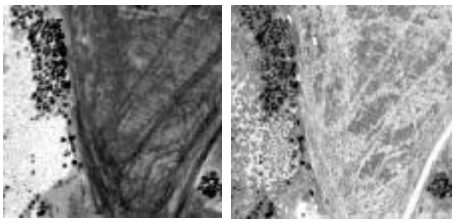

Channel Three

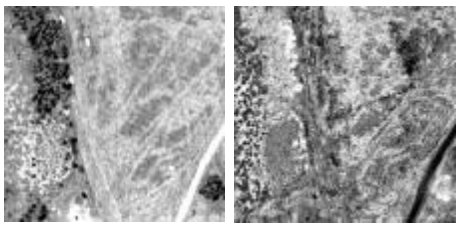

Channel Four

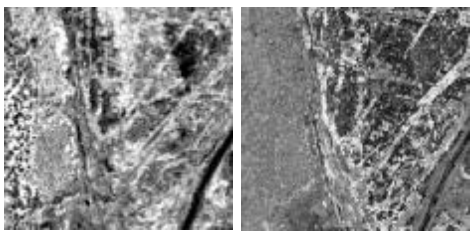

Channel Five

Figure 2: Dimension reduction results from Tucker decomposition (left panels) and PCA (right panels). The first five spectral components are shown here (AisaEAGLE)

A comparison of different target detection algorithms is done as shown in Table 1. Of the three algorithms NSW-DW (Liu and Chang 2004), is the most time consuming. Since ground truth is available, comparison on the recall rate, precision, accuracy and false alarm rate is carried out and results are as indicated in Table 1. Further, Figure shows the best detected image by RXD, four vehicles could be correctly identified (circled in the image), while the detection result by NSW is far from the ground truth. The reason for NSW-DW's underperformance is that the window size needs to be specified by estimating the target's size, however, the targets' dimensions vary and they are not strictly square.

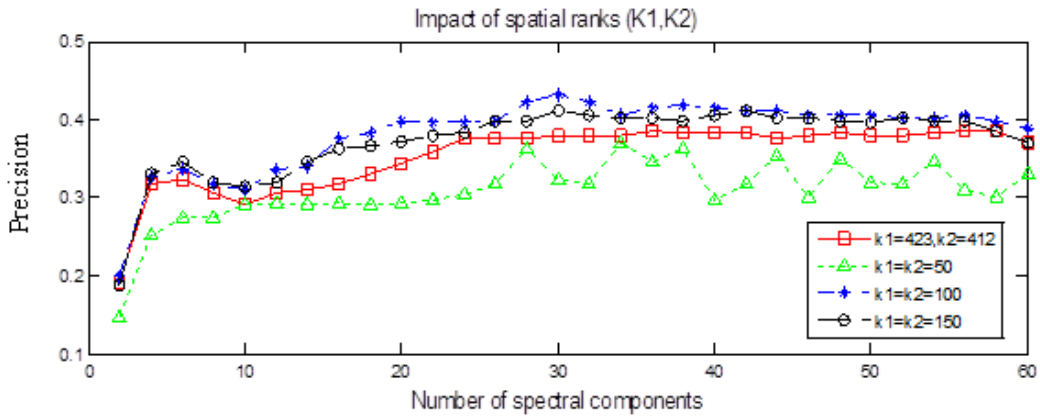

Figure 3. Impact of spatial ranks as a function of the number of spectral components for Tucker decomposition

Table 1. Comparison of the performance of different target detection algorithms

Algorithm	Recall Rate	Precision	Accuracy	False Alarm	Targets	Time (s)
RXD	0.3791	0.3333	0.9976	0.0013	4	2.15
RX-UTD	0.3725	0.3276	0.9976	0.0013	4	2.37
NSW	0.1242	0.1092	0.9967	0.0018	1	216.51

The RX detection algorithm was applied to both PCA and Tucker containing the first 30 spectral bands and their detection accuracy was compared against RXD applied on to the original hyperspectral image having 60 spectral bands. Results in Table 2 indicate that both Tucker and PCA perform better than the original image although the number of bands utilized was reduced by half. Tucker decomposed images are found to have better detection accuracy when compared to PCA at the expense of increased computational complexity. The redundancies contained within the hyperspectral image have been compressed utilizing dimension reduction algorithms without any loss of information. But the reduction in the spectral bands does not necessary result in a reduction in the computational complexity, as indicated by the time required for individual process the table. This is due to the high computational cost associated with the dimension reduction algorithm, especially with the case of Tucker decomposition. The reason for the detection of four targets out of six is because for camouflaged vehicles visual bands fail to yield much information to distinguish the target from its background.

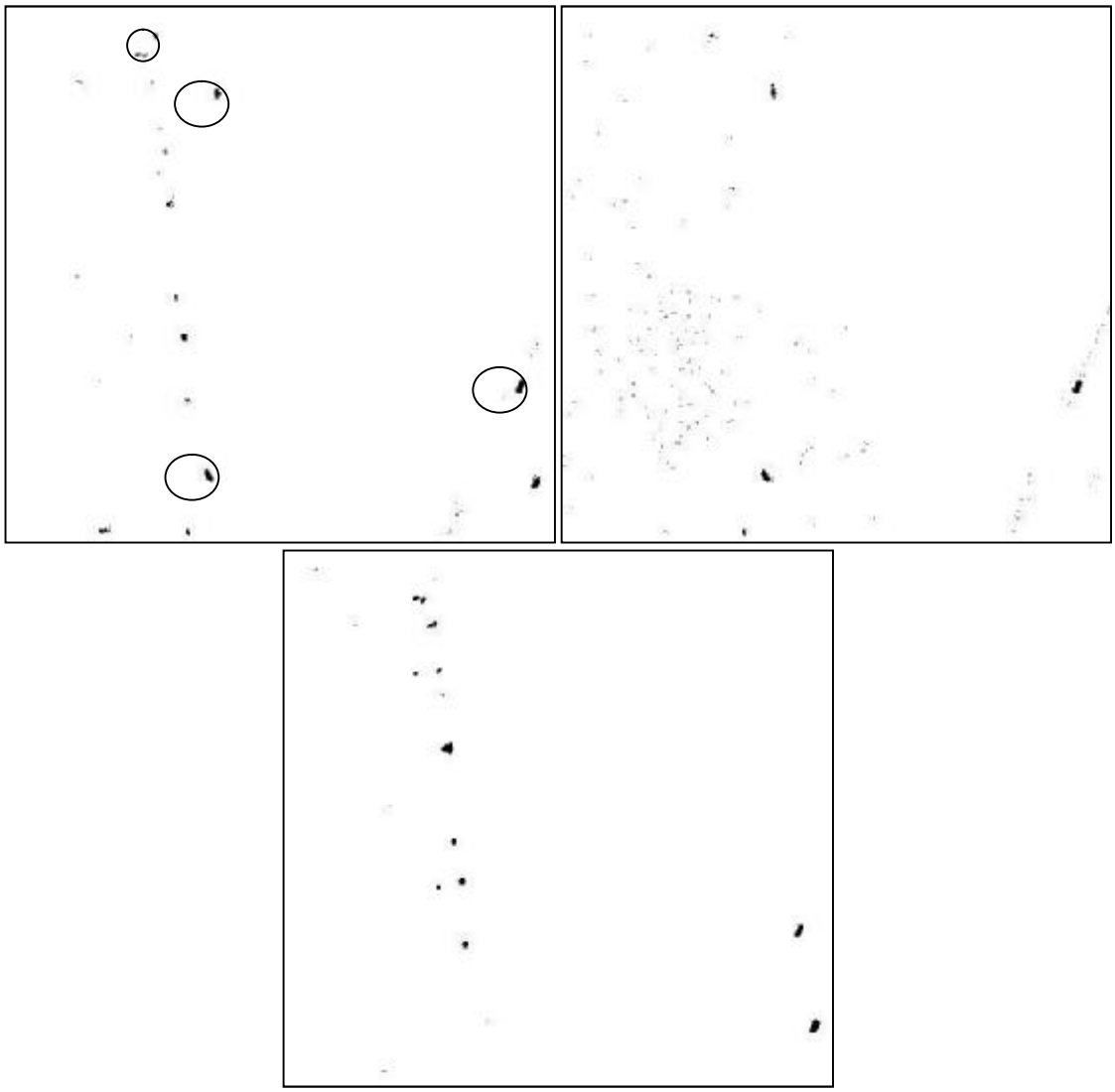

Figure 4. Vehicle detection results by different algorithms: Up left-RXD; up right-RXD-UTD; bottom-NSW-DW

Table 2: Comparison of vehicle detection results between raw images and images after dimension reduction

Image	Recall Rate	Precision	Accuracy	False Alarm	Targets	Time(s)
Raw	0.3791	0.3333	0.9976	0.0013	4	2.15
PCA (30 bands)	0.3954	0.3477	0.9976	0.0013	4	2.28
Tucker (30 bands)	0.4346	0.3822	0.9978	0.0012	4	18.56

5. CONCLUSIONS

In this work, we have shown the impact of dimension reduction using Tucker decomposition on target detection. A comparison of target detection accuracy was made on images whose dimensions were reduced using Tucker and PCA. Results indicate that compared to PCA, Tucker decomposition leads to better detection at the expense of time. We have also shown that out of the three detection algorithms employed, namely RXD, RXD-UTD and NSW,

RXD performs the best in terms of accuracy and computation time. In future, we plan to tackle the issue of computational complexity so as to enable a real-time implementation in an embedded platform.

REFERENCES:

Ashton, E. A. and Schaum, A., 1998. Algorithms for the detection of sub-pixel targets in multispectral imagery. Photogram Eng. Remote Sensing. 64(7), pp 723-731.

Chang, C.-I., Chiang, S.-S, 2002. Anomaly detection and classification for hyperspectral imagery. IEEE Transactions on Geoscience and Remote Sensing. 40(6), pp.1314 - 1325.

Farrell, M. D. and Mersereau, R. M., 2005. On the impact of PCA dimension reduction for hyperspectral detection of difficult targets. IEEE Geoscience and Remote Sensing Letters, 2 (2), pp. 192-195.

Landgrebe, D., 2002. Hyperspectral image data analysis as a high dimensional signal problem. Special issue of IEEE Signal processing Magazine, 19 (1), pp. 17-28.

Karami, Yazdi, M., and Zolghadr, A., 2011a. Noise reduction of hyperspectral images using kernel non-negative Tucker decomposition. IEEE Journal of Selected Topics In Signal Processing, 5 (3), pp. 487-493.

Karami, Yazdi M., and Zolghadr, A., 2012b. Compression of hyperspectral images using discrete wavelet transform and Tucker decomposition. IEEE Journal of Selected Topics In Applied Earth Observations and Remote Sensing. 5 (2), pp. 444-450.

Lathauwer, L. De, Moor, B. De, and Vandewalle, J. 2000. On the best rank (R_1, R_2…R_M) approximation of higher-order tensors. SIAM Journal on matrix Analysis and Applications. 21(4), pp. 1324-1342.

Liu, W. and Chang, C.–I. 2004. A nested spatial window based approach to target detetcion for hyper spectral imagery. IEEE International Geoscience and Remote Sensing Symposium. 1, 266-268.

Manolakis D., Lockwood R., Cooley, T. and Jacobson, J., 2009. Is there a best hyperspectral detection algorithm?. Algorithms and Technologies for Multispectral, Hyperspectral, and Ultraspectral Imagery XV. Ed. Sylvia S. Shen & Paul E. Lewis. Orlando, FL, USA: SPIE. 733402-16.

Manolakis, D., and Shaw, G., 2002. Detection algorithms for hyperspectral imaging application. IEEE Trans. Signal Processing. 19(1), pp. 29-43.

Reed, I.S. and Yu, X. 1990. Adaptive multiple-band CFAR detection of an optical pattern with unknown spectral distribution. IEEE Trans. Acoustics, Speech and Signal Processing, 38(10), pp.1760-1770.

Renard, N. and Bourennane, S., 2008. An ICA-based multilinear algebra tools for dimensionality reduction in hyperspectral imagery. in Proc. IEEE International Conference on Acoustics, Speech and Signal Processing, 19, pp. 1345-1348.

Stein, D.W.J., Beaven, S.G., Hoff, L.E., Winter, E.M., Schaum, A.P., and Stocker, A.D., 2002. Anomaly detection from hyperspectral imagery. IEEE Trans. Signal Processing Magazine. 19(1), pp. 58-69.

Tucker, L. R., 1966. Some mathematical notes on three-mode factor analysis. Psychometrika. 31(3), pp.279-311.

Wadstromer, N., Ahlberg, J. and Svensson, T., 2010. A new hyperspectral dataset and some challenges. Algorithms and Technologies for Multispectral, Hyperspectral and Ultraspectral Imagery XVI, SPIE. (7695), pp. 29-43.